

Ultra-low-loss ohmic contacts on heavily doped n-type InGaAs and InGaAsP for InP based photonic membranes

L. Shen,^{1,*} P.J. van Veldhoven,² Y. Jiao,¹ V. Dolores-Calzadilla,¹
J.J.G.M. van der Tol,¹ G. Roelkens,^{1,3} and M.K. Smit,¹

¹Photonic Integration Group, Eindhoven University of Technology, 5600 MB Eindhoven, The Netherlands

²Nanolab@TU/e, Eindhoven University of Technology, 5600 MB Eindhoven, The Netherlands

³Photonics Research Group, Ghent University-IMEC, B-9000 Ghent, Belgium

*L.shen@tue.nl

Abstract: We present AgGe based ohmic contacts to InP membranes with significantly reduced optical losses and contact resistances. Thanks to the high solubility of Si in InGaAs and InGaAsP, heavily doped n-type contact layers are grown on InP wafers. This high doping concentration gives rise to annealing-free ohmic contacts and low contact resistances in the level of $10^{-7} \Omega \text{ cm}^2$. It also leads to strong bandfilling effects in InGaAs and InGaAsP, which result in low optical absorption losses in the contact layer. Combined with the low optical loss of AgGe, a massive reduction of the propagation loss in membrane waveguides is observed compared with other existing solutions. An additional advantage is the minimal influence of thermal treatments during the processing, leading to very stable high performing contacts.

© 2015 Optical Society of America

OCIS codes: (130.3130) Integrated optics materials, (160.3900) Metals.

References and links

1. M. Smit, J. van der Tol, and M. Hill, "Moore's law in photonics," *Laser & Photon. Rev.* **6**(1), 1–13 (2012).
2. G. Roelkens, L. Liu, D. Liang, R. Jones, A. Fang, B. Koch, and J. Bowers, "III-V/silicon photonics for on-chip and intra-chip optical interconnects," *Laser & Photon. Rev.* **4**(6), 751–779 (2010).
3. J. van der Tol, R. Zhang, J. Pello, F. Bordas, G. Roelkens, H. Ambrosius, P. Thijs, F. Karouta, and M. Smit, "Photonic integration in indium-phosphide membranes on silicon," *IET Optoelectron.* **5**(5), 218–225 (2011).
4. S. Arai, N. Nishiyama, T. Maruyama, and T. Okumura, "GaInAsP/InP membrane lasers for optical interconnects," *IEEE J. Sel. Top. Quantum Electron.* **17**(5), 1381–1389 (2011).
5. M. Heck, J. Bauters, M. Davenport, J. Doylend, S. Jain, G. Kurczveil, S. Srinivasan, Y. Tang, and J. Bowers, "Hybrid silicon photonic integrated circuit technology," *IEEE J. Sel. Top. Quantum Electron.* **19**(4), 6100117 (2013).
6. L. Shen, V. Dolores-Calzadilla, C. Wullems, Y. Jiao, A. Millan-Mejia, A. Higuera-Rodriguez, D. Heiss, J. van der Tol, H. Ambrosius, G. Roelkens, and M. Smit, "Low-optical-loss, low-resistance Ag/Ge based ohmic contacts to n-type InP for membrane based waveguide devices," *Opt. Mater. Express* **5**(2), 393–398 (2015).
7. D. G. Ivey, D. Wang, D. Yang, R. Bruce, and G. Knight, "Au/Ge/Ni ohmic contacts to n-type InP," *J. Electron. Mater.* **23**(5), 441–446 (1994).
8. T. C. Shen, G. B. Gao, and H. Morko, "Recent developments in ohmic contacts for III-V compound semiconductors," *J. Vac. Sci Technol. B* **10**(5), 2113–2132 (1992).
9. M. H. Ettenberg, M. J. Lange, A. R. Sugg, M. J. Cohen, and G. H. Olsen, "Zinc diffusion in InAsP/InGaAs heterostructures," *J. Electron. Mater.* **28**(12), 1433–1439 (1999).
10. T. F. Kuech, B. S. Meyerson, and E. Veuhoff, "Disilane: A new silicon doping source in metalorganic chemical vapor deposition of GaAs," *Appl. Phys. Lett.* **44**(10), 986–988 (1984).

11. G. S. Marlow and M. B. Das, "The effects of contact size and non-zero metal resistance on the determination of specific contact resistance," *Solid-State Electron.* **25**(2), 91–94 (1982).
12. Logeeswaran VJ, N. P. Kobayashi, M. S. Islam, W. Wu, P. Chaturvedi, N. X. Fang, S. Y. Wang, and R. S. Williams, "Ultrasoother silver thin films deposited with a germanium nucleation layer," *Nano Lett.* **9**(1), 178–182 (2009).
13. A. Higuera-Rodriguez, V. Dolores-Calzadilla, Y. Jiao, E. J. Geluk, D. Heiss, and M. Smit, "Realization of efficient metal grating couplers for membrane-based integrated photonics," *Opt. Lett.* **40**(12), 2755–2757 (2015).
14. B. Bennett, R. A. Soref, and J. del Alamo, "Carrier-induced change in refractive index of InP, GaAs and InGaAsP," *IEEE J. Quantum Electron.* **26**(1), 113–122 (1990).
15. J.-P. Weber, "Optimization of the carrier-induced effective index change in InGaAsP waveguides-application to tunable Bragg filters," *IEEE J. Quantum Electron.* **30**(8), 1801–1816 (1994).
16. D. Hahn, O. Jaschinski, H. Wehmann, A. Schlachetzki, and M. Ortenberg, "Electron-concentration dependence of absorption and refraction in n-In_{0.53}ga_{0.47}as near the band-edge," *J. Electron. Mater.* **24**(10), 1357–1361 (1995).
17. A. Sneh, and C. Doerr, "InP-based photonic circuits and components," in *Integrated Optical Circuits and Components: Design and Applications*, E. Murphy, ed. (CRC Press, 1999).
18. S.-i. Gozu, T. Mozume, and H. Ishikawa, "Refractive index of Si-doped n-InGaAs," *J. Appl. Phys.* **104**(7), 073507 (2008).
19. H. G. Bukkems, Y. S. Oei, U. Richter, and B. Gruska, "Analysis of III-V layer stacks on INP substrates using spectroscopic ellipsometry in the NIR spectral range," *Thin Solid Films* **364**(1–2), 165–170 (2000).
20. Y. Jiao, J. Pello, A. Millan-Mejia, L. Shen, B. Smalbrugge, E. J. Geluk, M. Smit, and J. van der Tol, "Fullerene-assisted electron-beam lithography for pattern improvement and loss reduction in InP membrane waveguide devices," *Opt. Lett.* **39**(6), 1645–1648 (2014).
21. Y. Jiao, T. d. Vries, R. Unger, L. Shen, H. Ambrosius, C. Radu, M. Arens, M. Smit, and J. van der Tol, "Vertical and smooth single-step Reactive Ion Etching process for InP membrane waveguides," *J. Electrochem. Soc.* **162**(8), E90–E95 (2015).
22. W. Spitzer, and J. Whelan, "Infrared absorption and electron effective mass in n-type Gallium Arsenide," *Phys. Rev.* **114**(1), 59–63 (1959).

1. Introduction

In the last decade membrane photonics emerges as a promising platform technology for hybrid integration of III-V materials with Si chips [1–5]. It also brings new technological challenges for fabricating devices with good performances. For example, ohmic contacts with good electrical and optical properties become critical when they are placed on top of membrane devices. On the one hand, their contact resistances need to be minimized to obtain high bandwidth and low power consumption. On the other hand, low optical loss from these contacts is required for devices integrated in a membrane with only sub-micron thickness.

Recently we developed a new AgGe based contact solution to InP based membranes bonded on top of Si wafers [6]. Promising electrical and optical properties were demonstrated by contacting AgGe to n-type doped InP. The role of Ge in forming an n-type ohmic contact was observed and its thickness was optimized to reach the minimal contact resistance. Compared with the conventional AuGeNi based n-type contacts [7], this approach shows much lower optical loss in the telecommunication wavelength range due to the absence of Ni which has a high absorption coefficient and a high refractive index. Moreover, by replacing Au with Ag, the thermal stability of the metal contact is improved due to a higher eutectic temperature of the AgGe alloy compared with that of AuGe. Therefore the well-known spiking effect in Au based contacts during a thermal annealing process is significantly reduced in the Ag based solution [8]. However, the contact resistance of AgGe based contacts remains one order of magnitude higher than that of AuGeNi based ones. Furthermore, a certain amount of increase of the optical loss after annealing is observed. Possible reasons include interface degradation due to spikes in the Ge layer, Ge diffusion into the InP layer, and degradation of the polymer-based bonding layer below the membrane.

In this paper, we present a significant improvement to reduce both the contact resistance and the optical loss. InGaAs and InGaAsP are used as contact layers between the AgGe contact and the InP waveguide (WG) layers. They are grown with Metalorganic Chemical Vapor De-

position (MOCVD) at 650 °C using disilane as the doping gas source. The solubility of Si in the ternary and quaternary alloys is known to be much higher than that in InP [9]. Also, disilane has a higher decomposition reaction efficiency at 650 °C than silane which was used previously [10]. Consequently, these contact layers can be doped with electron concentrations of more than 10^{19} cm^{-3} , which is one order of magnitude higher than that of the InP contact layer in the previous work. By using these heavily doped materials, ohmic contacts between AgGe and the contact layers can be formed without any annealing process. Electrical measurements show that their specific contact resistances can be minimized to the same level of those in conventional AuGeNi/InP contacts. Furthermore, the thickness of the Ge layer, which was suggested to be the origin of the increase of the WG propagation loss after annealing [6], can be dramatically reduced while maintaining a low contact resistance. In terms of optical properties, the added contact layers show low absorption losses due to a strong bandfilling effect in these heavily n-type doped materials. Optical propagation losses from these contacts are measured with membrane WGs before and after annealing. A factor of 3 reduction of the propagation loss is obtained compared to the values measured from AgGe/InP contacts [6].

2. Specific contact resistance

For the measurement of the specific contact resistances, two samples are prepared containing an n-InGaAs contact layer and an n-InGaAsP contact layer, respectively. The InGaAsP quaternary alloy has a bandgap wavelength of 1.25 μm (hereafter referred to as Q1.25). These contact layers are 100 nm thick and are grown on top of Fe-doped semi-insulating InP (100) substrates using MOCVD. Disilane is used as the doping gas source. The doping concentrations are characterized using an electrochemical C-V profiler, yielding $2 \times 10^{19} \text{ cm}^{-3}$ and $5 \times 10^{19} \text{ cm}^{-3}$ for n-InGaAs and n-Q1.25, respectively. It should be taken into account however that the relative error in the C-V measurement can be up to 50%. The circular transfer length method (CTLTM) is used to characterize the specific contact resistance [11]. Metal patterns are defined using optical lithography and a lift-off process. Before metal deposition, the samples are cleaned in an oxygen plasma (50 W, 5 minutes), followed by dipping in a $\text{H}_3\text{PO}_4:\text{H}_2\text{O}$ (1:10) solution for 2 minutes. After these surface treatments, a layer of Ge is deposited on top of the contact layer using electron beam evaporation, followed by deposition of 300 nm of Ag. Samples are measured both before and after annealing, for which a rapid thermal process at 400 °C for 15 seconds is performed.

Table 1. Specific contact resistances

Metals	Contact material and doping level (cm^{-3})	Thickness Ge (nm)	Specific contact resistance ($\Omega \text{ cm}^2$)	
			Before annealing	After annealing
AgGe	InGaAs: 2×10^{19}	2	7.2×10^{-7}	1.4×10^{-7}
		15	Non-Ohmic	1.9×10^{-7}
AgGe	Q1.25: 5×10^{19}	2	2.4×10^{-7}	4.4×10^{-8}
		15	Non-Ohmic	4.2×10^{-8}
AgGe	InP: 2×10^{18}	2	5.6×10^{-4}	2.6×10^{-5}
		30	Non-Ohmic	1.5×10^{-6} [6]
AuGeNi	InP: 2×10^{18}	50	Non-Ohmic	1.0×10^{-7} [7]

The measured specific contact resistances are summarized in Table 1. For comparison, the optimal values obtained from AgGe/InP contacts and from conventional AuGeNi/InP contacts are also shown. Before annealing, samples with a 2 nm Ge layer show ohmic behavior. After annealing, the contact resistances reduce to a level comparable to or even lower than the

values from the conventional low-resistance AuGeNi/InP contact. Samples with Q1.25 contact layer provide a lower contact resistance compared with the ones with InGaAs, which can be attributed to the higher doping level in Q1.25. The dependence of the contact resistance on the Ge thickness observed in previous works is not obvious in these highly doped contacts, suggesting that the contribution of Ge to the doping in the contact surface is not important in a contact layer with such a high doping level. The remaining 2 nm Ge mainly serves as a nucleation layer to improve the adhesion and the surface quality of the Ag layer [12, 13]. The reduction of the Ge thickness will benefit the optical properties, as will be discussed in Section 4.

The ohmic behavior observed before annealing is assumed to result from the tunnelling current through the thin barrier of the 2 nm Ge layer. The current flow in heavily doped semiconductor contacts is governed by the field emission mechanism, for which the specific contact resistance depends strongly on the doping concentration [8]. Consequently, the high doping concentration in the contact layer of Q1.25 leads to a very low specific contact resistance ($2.4 \times 10^{-7} \Omega \text{ cm}^2$), which is almost one order of magnitude lower than the minimal value from the annealed AgGe/InP contact [6]. This annealing-free low-resistance contact is highly desirable in membrane photonic devices, as it fundamentally avoids any high temperature related degradation of the optical properties.

3. Optical properties of highly doped InGaAs and Q1.25

In this section, the effects which will influence the optical absorption and the refractive index of InGaAs and Q1.25 with high doping concentrations will be described, supplemented by experimental results on material absorptions.

3.1. Carrier induced change in material absorption

In order to evaluate the optical performance of the newly developed contacts, the optical loss introduced by the InGaAs and Q1.25 contact layers need to be studied first. This is particularly important for InGaAs, which has a bandgap of 0.74 eV, smaller than the photon energy in the telecommunication wavelength range. Therefore intrinsic InGaAs is extensively used as the absorption material in 1.55 μm photodetectors. In n-type heavily doped semiconductors, however, a reduction of absorption near the bandgap is a well-known phenomenon, which has been explained by the bandfilling effect [14]. That is, the energy states at the bottom of the conduction band are filled by the high concentration of free electrons, so that photons need energies higher than the bandgap energy to excite an electron from the valence band to the conduction band. This effect is particularly strong in n-type materials owing to the smaller effective mass of electrons and the lower density of states. In this paper, a model proposed by Weber is used [15], including mainly three free-carrier induced effects: bandfilling (BF), bandgap shrinkage (BS), and free carrier absorption (FCA). This model is originally used to study the carrier-injection related effects. It should also be applicable to doped materials by calculating the Fermi level shift due to free electrons, instead of calculating the quasi-Fermi levels for the conduction band and the valence band under injection. In this model, the interband absorption coefficient from an undoped direct-bandgap semiconductor is given by

$$\alpha(E) = \begin{cases} CE^{-1}(E - E_g)^{1/2}, & E > E_g \\ 0, & E < E_g \end{cases} \quad (1)$$

where E and E_g are the photon energy and the bandgap energy, respectively. The constant C is a material constant determined from measurement data. It should be noted that parabolic bands are assumed and that the Urbach tail is neglected in this equation. In this model, the bandfilling effect is considered based on a narrowed bandgap. To be more specific, free carriers are first

modeled as a cause for bandgap shrinkage, followed by their filling of the new band structure:

$$\alpha_{BF,BS} = \alpha(E - \Delta E_g)[f(E_v) - f(E_c)], \quad (2)$$

where ΔE_g is the shrank bandgap energy. E_v and E_c are the energies in the valence band and the conduction band, respectively, between which the interband transition takes place. They can be calculated by applying energy and momentum conservations. Heavy holes and light holes are both considered in the calculation. f indicates the probability of a state of energy occupied by an electron, which is described by the Fermi-Dirac distribution function:

$$f(E_{v,c}) = \left[1 + \exp\left(\frac{E_{v,c} - E_F}{k_B T}\right) \right]^{-1}, \quad (3)$$

where k_B is Boltzmann's constant and T is absolute temperature. E_F is the carrier dependent Fermi level in doped semiconductors which can be calculated by the Nilsson approximation [14]. For highly doped (degenerate) n-type semiconductors, the Fermi level is usually a few $k_B T$ into the conduction band. In this case, $f(E_v)$ is almost equal to 1. $f(E_c)$ increases with an increasing electron concentration and approaches to 1, indicating a reduction of the absorption coefficient. Details about the calculation can be found in [15].

By applying this model to InGaAs at a wavelength of 1.55 μm , it predicts a steep drop of the absorption coefficient for electron concentrations higher than 10^{18} cm^{-3} [see Fig. 1(a)], as a result from the dominant bandfilling effect. Experimental data from [16] show a reasonable agreement with this decreasing trend. Comparisons with measurement results from our samples will be discussed in Section 3.3.

Apart from the interband absorption, free carrier absorption is also taken into account. In n-type InP related materials, the free electron absorption is usually very low in the telecommunication wavelength range. However, it is assumed to be proportional to the electron concentration, implying a stronger effect in very heavily doped materials. A linear relation between the electron concentration and the resulting absorption coefficient at 1.55 μm is proposed in [17]:

$$\alpha_{FCA} = A \times 10^{-18} N_e, \quad (4)$$

where N_e indicates the electron concentration in cm^{-3} . The value of constant A is estimated to be between 1 and 2 (cm^2), based on measured data from different InGaAsP alloys with a bandgap wavelength from 1 μm to 1.3 μm . This bandgap range covers Q1.25 but not InGaAs. Nevertheless we use the mean value of 1.5 (cm^2) as an approximation of the constant A in our model for both InGaAs and Q1.25. The contribution from the free carrier absorption is shown in Fig. 1(a) as the rise of the InGaAs curve beyond 10^{19} cm^{-3} .

In terms of Q1.25, the absorption changes due to bandfilling and bandgap shrinkage are not visible till a electron concentration of 10^{20} cm^{-3} , owing to its much larger initial bandgap energy compared with the photon energy of 1.55 μm . Instead of interband absorption, the free carrier absorption is the dominant loss source in n-Q1.25.

3.2. Carrier induced change in refractive index

The change in the refractive index is related to the absorption change induced by bandfilling and bandgap shrinkage, which is described by the Kramers-Kronig integral:

$$\Delta n(E)_{BF,BS} = 2c\hbar P \int_0^\infty \frac{\Delta\alpha(E')_{BF,BS}}{E'^2 - E^2} dE', \quad (5)$$

where c , \hbar , and P indicate the speed of light, the reduced Plank constant, and the principal value of the integral. $\Delta\alpha(E)_{BF,BS}$ is calculated by subtracting Eq. (2) by Eq. (1). The index change due

to the free carrier absorption (also known as the plasma effect) is calculated separately [14, 15]. For n-type materials,

$$\Delta n_{FCA} = -\frac{6.893 \times 10^{-28}}{n_0 E^2 m_e^*} N_e, \quad (6)$$

where n_0 is the index of the undoped material, and m_e^* is electron effective mass. The total index change is the sum of these two effects, and the resultant refractive index is therefore

$$n = n_0 + \Delta n_{BF,BS} + \Delta n_{FCA}. \quad (7)$$

The calculated refractive indices of InGaAs and Q1.25 are plotted in Fig. 2(b). Both of them reduce at the high doping range. Experimental data on n-InGaAs can be found in [18]. Our samples are characterized using spectroscopic ellipsometry [19], giving refractive indices of 3.51 and 3.20 for InGaAs (Sample A) and Q1.25 (Sample B), respectively. The error of these measured results are estimated to be ± 0.02 as indicated by the vertical error bar. It originates from the surface roughness and oxidation of the samples. Even though the decreasing trend in all these experimental data is evident, its magnitude deviates from the model. According to [18], the overestimation of the index reduction in the model is assumed to be a result from the neglected conduction band nonparabolicity and the Urbach tail near the bandgap. It seems to be impractical to precisely quantify these two missing effects in the model due to the lack of accurate experimental data. The reduced refractive index in the contact layer will also help to reduce the optical loss as the mode will be more confined in the WG layer and will have less overlap with the metal contact on top. This effect is however very limited due to the relatively small reduction of the index.

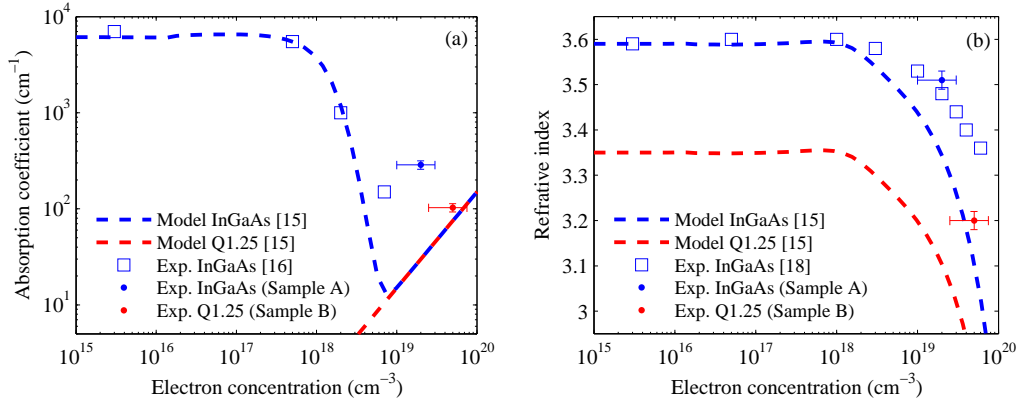


Fig. 1. (a) Absorption coefficient and (b) Refractive index of InGaAs and Q1.25 at 1.55 μm as a function of electron concentration. Both modeling and experimental data are included.

3.3. Waveguide measurements of absorption from InGaAs and Q1.25

Although the model introduced in Section 3.1 predicts low optical absorption from both highly doped n-InGaAs and n-Q1.25, existing experimental data are very limited in the high doping range. The only data we can find for n-InGaAs [16] are measured using transmission spectroscopy from LPE grown layers with thickness inhomogeneities. The minimal absorption coefficient that could be measured is 300 cm⁻¹. As lower optical absorption in the contact layer is essential, our MOCVD grown contact layers need to be characterized to give an accurate value of the absorption coefficient.

Standard optical loss measurements using membrane WGs fabricated in our platform (InP Membranes on Silicon, IMOS [3]) have been demonstrated with very high accuracy and resolution for the determination of the optical loss coefficient. Details of the fabrication process and the measurement setup can be found in [20, 21]. Fig. 2(a) shows the schematic cross-section of the WG structure used in this work. The WG contains a 250 nm undoped InP layer and a 50 nm contact layer on top. Two samples (Sample A and Sample B) are fabricated with n-InGaAs and n-Q1.25, respectively, as the contact layer. Their doping concentrations are the same as mentioned in Section 2. The WG array used in the loss measurements [see Fig. 2(b)] consists of WGs with a fixed width ($10\ \mu\text{m}$) and various lengths (ranging from $400\ \mu\text{m}$ to $1300\ \mu\text{m}$). Grating couplers on both sides of the WG are fabricated to couple the TE polarized WG mode with single-mode fibers placed of an angle of 9° from the normal direction to the surface of the sample. A commercial laser with a tunable wavelength ranging from $1.52\ \mu\text{m}$ to $1.63\ \mu\text{m}$ is used in this measurement.

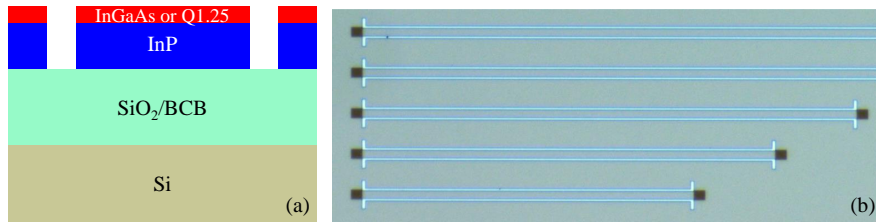


Fig. 2. (a) Schematic cross-section of a membrane WG with a contact layer on top. (b) Microscope image of an array of the fabricated WGs of various length. The dark parts at both ends of each WG are the grating couplers

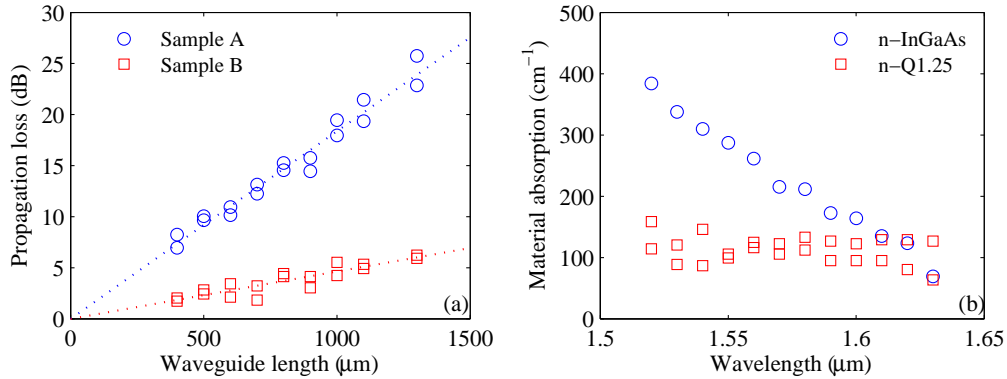


Fig. 3. (a) Propagation loss (at $1.55\ \mu\text{m}$) of membrane WGs in Sample A and B as a function of WG length. Dotted lines represent linear fits. (b) Material absorption coefficient of n-InGaAs and n-Q1.25 as a function of wavelength, obtained from Sample A and B respectively.

Insertion loss (including both propagation loss from WGs and coupling loss from gratings) from WGs of different lengths is measured, followed by a linear fitting. The normalized data at a input wavelength of $1.55\ \mu\text{m}$ are plotted in Fig. 3(a), showing the propagation loss from the WGs in Sample A and B as a function of the WG length. Clearly the WGs with n-Q1.25 as the contact layer produce lower loss compared to the ones with n-InGaAs. From the linear

fitting the propagation loss coefficients from the WGs in the two samples can be extracted. With these modal absorption coefficients, simulations based on a vectorial mode solver can be performed to calculate the material absorption coefficient of the contact layer. The refractive indices measured in Section 3.2 are used in the simulations. Given the uncertainties in the measured indices and in the thickness of the grown layers, an error of up to 10% is estimated in the results. The calculated material absorption coefficients from measurements at different wavelengths are plotted in Fig. 3(b). At $1.55 \mu\text{m}$ the absorption coefficients of n-InGaAs and n-Q1.25 are 287 cm^{-1} and 103 cm^{-1} , respectively. While the absorption of n-Q1.25 is close to the trend of the modeling result in Fig. 1(a), the value of n-InGaAs is almost one order of magnitude higher compared to the modeling result. This could indicate an overestimation of the bandfilling effect in the model we used. It can also be seen from Fig. 3(b) that the absorption of n-InGaAs drops with increasing wavelength, which is a typical behavior of interband absorption. This remaining interband absorption could be related to the unfilled energy states in the conduction band, for which the amount is underestimated in the model. In contrast, the absorption coefficient of n-Q1.25 does not show a clear wavelength dependence, which is a typical free carrier absorption dominant behavior in n-type III-V materials at this wavelength range [22]. Considering the lower value of both the material absorption and the refractive index, n-Q1.25 should be the better choice as the contact layer material.

4. Propagation loss from metal contacts

After the characterizations of the material loss of the contact layer with membrane WGs, the propagation loss from metal contacts are measured using the same WGs. Based on the electrical measurement results in Section 2, metal contacts with 2nm Ge and 300 nm Ag are chosen, since they provide annealing-free ohmic contacts with sufficiently low contact resistance. They are patterned on top of the WGs using electron beam lithography and a lift-off process. Afterwards, the contact layer of InGaAs (in Sample A) and Q1.25 (in Sample B) are removed with a selective etching solution of $\text{H}_2\text{SO}_4:\text{H}_2\text{O}_2:\text{H}_2\text{O}$ (1:1:10) using the metal contacts as masks. The schematic cross-section of the resulting structure can be seen in Fig. 4(a). The width of metal contacts is designed as $7 \mu\text{m}$, slightly smaller than the WG width ($10 \mu\text{m}$), to avoid metal covering of the side-walls of the WGs. Metal contacts with varying lengths deposited on top of WGs with a fixed length are measured [see Fig. 4(b)]. The same measurement approach from Section 3.3 is used here to obtain the propagation loss from the metal contacts together with the contact layers. The results are plotted in Fig. 5. The corresponding propagation loss coefficients extracted from the linear fitting are shown in Table 2. In addition, we also compare with the results from AuGeNi/InP and AgGe/InP contacts after thermal annealing (which is essential for forming ohmic contacts there) [6].

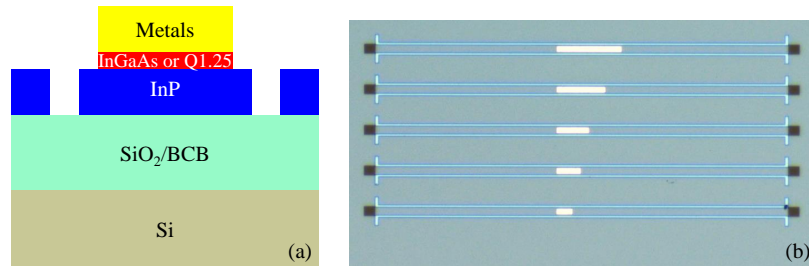


Fig. 4. (a) Schematic cross-section of a membrane WG with metal contact on top. (b) Microscope image of an array of the fabricated WGs with metal contacts of various length.

Without annealing, both ohmic contacts in Sample A and B show very low propagation loss, which can be expected from the low-loss AgGe metal contacts. Sample B with Q1.25 as the contact layer gives a lower loss coefficient, which is reasonable considering the lower material absorption measured from n-Q1.25 compared with that from n-InGaAs. Compared with the values measured from AgGe/InP and AuGeNi/InP (ohmic contacts, with annealing), the loss coefficient from the AgGe/Q1.25 annealing-free ohmic contact is lower by a factor of 3 and 17, respectively. The comparison is reasonable as all of the WG structures used in the measurements are fabricated in one membrane platform with the same thickness of the semiconductor membrane (300 nm).

Furthermore, the samples measured in this work show only a slight increase (about 10%) of the propagation loss even after the standard thermal annealing process (400°C, 15 seconds), which is in strong contrast to previous samples. This may be related to the reduction of the Ge thickness in the new samples. According to our previous work [6], metal spikes were observed in the Ge layer after annealing, which could contribute to the propagation loss. Also, the diffusion of Ge could be a source of the increasing loss in the annealed contacts. However, the amount of Ge cannot be significantly reduced in ohmic contacts to n-InP in order to maintain a low contact resistance. In the present work, the Ge thickness can be reduced to only 2 nm thanks to the use of highly doped contact layers. Therefore, a better thermal stability and a larger thermal process window is obtained.

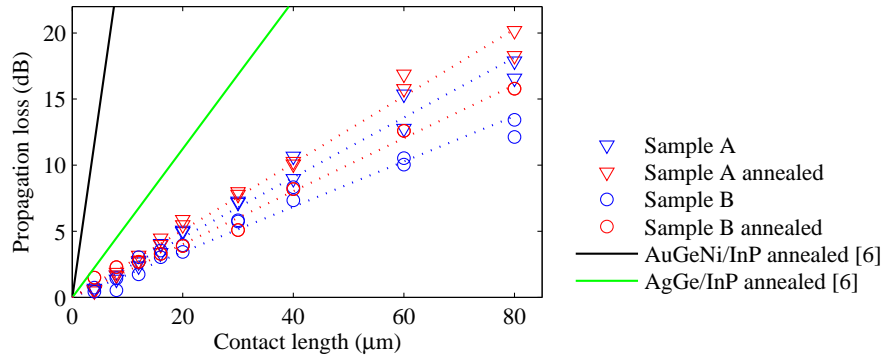


Fig. 5. Propagation loss (at 1.55 μm) of membrane WGs in Sample A and B as a function of the length of metal contact. Results obtained both before and after annealing are shown. Dotted lines represent linear fits. For comparison the results obtained from [6] are also included.

Table 2. Propagation loss coefficients (dB/ μm).

Contact type	Before annealing	After annealing	
AgGe/InGaAs	0.23	0.25	
AgGe/Q1.25	0.17	0.19	
AgGe/InP	0.18 ^a	0.56	[6]
AuGeNi/InP	0.93 ^b	2.91	[6]

^{a,b}These are not ohmic contacts without annealing

5. Conclusion

We have developed new n-type ohmic contacts based on AgGe to InGaAs and Q1.25 contact layers. These layers can be heavily doped in MOCVD to a level which is one order of magnitude higher than the maximum doping in InP, thanks to the higher solubility of Si. This high doping concentration, from the electrical point of view, provides annealing-free ohmic contacts with low contact resistances in the level of $10^{-7} \Omega \text{ cm}^2$. The optical properties of the highly doped contact materials are studied. Strong bandfilling effects are observed to result in low optical absorption loss in the contact layer. The annealing-free contacts have been tested with optical loss measurements using membrane WGs. Compared to previously demonstrated AgGe/InP ohmic contacts and conventional AuGeNi/InP ones, the new solution based on AgGe/Q1.25 shows reductions in the propagation loss of a factor of 3 and 17, respectively. Furthermore, the Ge thickness in this new solution can be reduced to only 2 nm, which results in better thermal stability of the contacts. These optimized ohmic contacts with ultra-low contact resistance and optical loss are expected to enable more advanced devices fabricated in membrane photonic platforms.

Acknowledgments

This work is supported by the ERC project NOLIMITS and the EU FP7 project NAVOLCHI. The authors acknowledge Nanolab@TU/e for the cleanroom facilities.